Available online at www.sciencedirect.com

SciVerse ScienceDirect

Geochimica et Cosmochimica Acta 100 (2013) 251–263

Geochimica et Cosmochimica Acta

www.elsevier.com/locate/gca

Experimental determination of rhyolitic glass dissolution rates at 40–200 °C and 2 < pH < 10.1

Julien Declercq [a], Tamara Diedrich [a], Melissa Perrot [a], Sigurdur R. Gislason [b], Eric H. Oelkers [a,*]

[a] GET–UMR 5563 CNRS Université Paul-Sabatier IRD, 14, avenue Edouard Belin, 31400 Toulouse, France
[b] Institute of Earth Sciences, University of Iceland, Sturlugata 7, 101 Reykjavik, Iceland

Received 19 October 2011; accepted in revised form 2 October 2012; available online 12 October 2012

Abstract

The steady-state dissolution rates of Öraefajökull rhyolitic glass were measured in titanium mixed-flow reactors as a function of aqueous Al, Si, and oxalic acid concentration at temperatures from 40 to 200 °C and pH from 2 to 10.1. Measured dissolution rates at were found to be consistent with

$$r_+ = Ae^{-\left(\frac{E_A}{RT}\right)}\left(\frac{a^3_{H^+}}{a_{Al^{3+}}}\right)^{1/n}$$

where r_+ refers to the specific dissolution rate, A represents a pre-exponential factor equal to 1.4×10^{-5} mol/cm^2/s, E_A denotes an activation energy equal to 55.15 kJ/mol, n represents a stoichiometric factor equal to 11.1, R designates the gas constant, T corresponds to the absolute temperature and a_i defines the activity of the subscripted aqueous species. In accord with this equation, aqueous organic ligands will enhance rates by complexing with aqueous Al^{3+}, thus lowering $a_{Al^{3+}}$. The observed variation of rhyolite dissolution rates with solution chemistry and temperature is similar to that previously observed for basaltic glass. This similarity suggests that all natural Al-silicate volcanic glasses have similar dissolution mechanisms consisting of the sequential removal of metals from the glass structure via proton exchange reactions. The overall dissolution rate within this mechanism is controlled by the detachment of Si tetrahedral that have been partially liberated from the glass structure through the removal of adjoining Al.

1. INTRODUCTION

Volcanic glass dissolution plays a major role in a variety of natural processes. Nearly 1 km^3 of glass is produced every year, mostly along the oceanic ridges (Morgan and Spera, 2001). Glass shards fall on land and on the seafloor within a few hours or days after an explosive eruption (Carey, 1997). Dispersal of airborne volcanic glass, primarily of silica-rich tephra, originating from explosive volcanic eruptions plays a significant role in sedimentary processes (Sparks et al., 1992; Larsen et al., 2001; Lacasse and van den Bogaard, 2002), and can be detrimental to the environment (Stewart et al., 2006; Flaathen and Gislason, 2007; Durant et al., 2010; Flaathen et al., 2010; Ruggieri et al., 2010; Wilson et al., 2010; Wall-Palmer et al., 2011). Volcanic glass releases divalent cations during its dissolution which can influence the long-term atmospheric CO_2 concentration (Urey, 1952; Riley and Chester, 1971; Holland, 1978; Berner et al., 1983; Spivack and Staudigel, 1994; Brady and Gislason, 1997; Chester et al., 2000; Kump et al., 2000; Wolff-Boenisch et al., 2006; Jones and Gislason, 2008) and can be used as a source material for mineral carbonation (Oelkers and Schott, 2005; McGrail et al., 2006; Marini, 2007; Oelkers et al., 2008; Gislason et al., 2010). Because of their high reactivity, the chemical weathering of

* Corresponding author.
E-mail address: oelkers@lmtg.obs-mip.fr (E.H. Oelkers).

0016-7037/$ - see front matter © 2012 Elsevier Ltd. All rights reserved.
http://dx.doi.org/10.1016/j.gca.2012.10.006

natural glass influences the global cycle of numerous elements (Gow and Williamson, 1971; Gislason et al., 1996, 2006, 2009; Brady and Gislason, 1997; Louvat and Allegre, 1997; Moulton et al., 2000; Dessert et al., 2001; Stefansson and Gislason, 2001; Arsouze et al., 2009; Jeandel et al., 2011; Oelkers et al., 2011).

In contrast to the plethora of studies focused on the dissolution rates of basaltic and borosilicate glasses (e.g. Guy and Schott, 1989; McGrail et al., 1997; Oelkers and Gislason, 2001; Techer et al., 2001; Gislason and Oelkers, 2003; Curti et al., 2006; Conradt, 2008; Icenhower et al., 2008; Pierce et al., 2010), relatively few studies have focused on acidic volcanic glasses (e.g. Fiore et al., 1999; Techer, 1999; Yokoyama and Banfield, 2002). Studies of acid volcanic and other silicate glass dissolution behaviour include work aimed at their potential utility as nuclear waste hosts (e.g. Kharkansis et al., 1980; Dickin, 1981; Petit, 1992; Shoesmith, 2000; Gin and Mestre, 2001; Rajmohan et al., 2010), and studies of their leaching behaviour in an effort to better understand their role in natural processes (White and Claassen, 1980; White, 1983; Allnatt et al., 1983; Dran et al., 1986, 1988; Magonthier et al., 1992; Mungall and Martin, 1994; Mazer and Walther, 1994; Fiore et al., 1999; Cailleteau et al., 2008). Building on these studies, the dissolution rates of Öraefajökull rhyolitic glass have been measured as a function of temperature and aqueous solution composition. The goal of this paper is to present the results of this experimental study and to use these results to illuminate the dissolution mechanism of natural glass.

2. THEORETICAL CONSIDERATION

The standard state adopted in this study is that of unit activity of pure minerals and H_2O at any temperature and pressure. For aqueous species other than H_2O, the standard state is unit activity of species in a hypothetical 1 M solution referenced to infinite dilution at any temperature and pressure. The activities of species present at glass surfaces are assumed to be equal to their mole fraction. All thermodynamic calculations in the present study were generated using the PHREEQC computer code (Parkhurst and Appelo, 1999) together with its llnl database after adding to it the equilibrium constants for aqueous oxalate and Al-oxalate species taken from Kettler et al. (1998) and Prapaipong et al. (1999), respectively.

Due to their similar compositions and structures it seems likely that the dissolution mechanism of rhyolitic glass is similar to that of basaltic glass and multi-oxide Al-silicate minerals. Dissolution is initiated by the removal of the metals having the fastest breaking metal–oxygen bonds by proton exchange reactions. Dissolution continues by the successive removal of metals in the order of the relative rates for breaking their corresponding metal–oxygen bonds, until the mineral or glass structure is destroyed. For the case of natural Al-silicate glasses, dissolution begins by the rapid exchange of protons for alkali and alkaline-earth metals near the glass surface leading to the formation of an Al and Si-rich surface layer (Thomassin and Touray, 1979; Berger et al., 1987; Guy and Schott, 1989; Crovisier et al., 1990, 2003; Gout et al., 1997; Oelkers et al., 2009). This surface layer attains a constant thickness within several hours (Guy and Schott, 1989; Crovisier et al., 1990), leading to long-term stoichiometric dissolution (Gislason and Eugster, 1987; Crovisier et al., 1992). The final and rate limiting step of natural aluminosilicate glass dissolution is the destruction of this Si and Al rich surface layer (Daux et al., 1997; Oelkers and Gislason, 2001; Gislason and Oelkers, 2003; Wolff-Boenisch et al., 2004a,b). Because the breaking of Al–O bonds is rapid compared to breaking of Si–O bonds (Oelkers, 2001), some Al is removed from this surface layer leading to the formation of partially detached Si tetrahedra. The removal of the partially detached Si from this leached layer constitutes the rate limiting step for the dissolution of numerous Al silicates. Partially detached Si are formed from the removal of adjacent Al atoms in accord with (Oelkers, 2001)

$$>(\mathrm{Si–O})_{\boldsymbol{n}}\text{–Al} + 3\mathrm{H^+} = \boldsymbol{n} > \mathrm{Si–O–H_{3/\boldsymbol{n}}} + \mathrm{Al^{3+}} \tag{1}$$

where $>\mathrm{Si–O–H_{3/\boldsymbol{n}}}$ represents a partially detached Si whereas $>(\mathrm{Si–O})_{\boldsymbol{n}}$–Al represents fully attached Si groups near the glass surface. The law of mass action for reaction (1) is given by

$$\boldsymbol{K}_1 = \frac{\boldsymbol{a}_{\mathrm{Al^{3+}}}\boldsymbol{X}^{\boldsymbol{n}}_{>\mathrm{Si–O–H_{3/\boldsymbol{n}}}}}{\boldsymbol{a}^3_{\mathrm{H^+}}\boldsymbol{X}_{>(\mathrm{Si–O})_{\boldsymbol{n}}\text{–Al}}} \tag{2}$$

where $\boldsymbol{K}_1$ corresponds to the equilibrium constant of reaction (1), $\boldsymbol{a}_i$ denotes the activity of the ith aqueous species, $\boldsymbol{n}$ refers to the number of partially detached Si created by the removal of one Al atom from the surface, and $\boldsymbol{X}_i$ stands for the mole fraction of the subscripted surface species. At conditions where the surface has retained most of its Al, $\boldsymbol{X}_{>(\mathrm{Si–O})\boldsymbol{n}\text{–Al}} \approx 1$, and,

$$\boldsymbol{X}_{>(\mathrm{Si–O})\text{–}\mathrm{H_{3/\boldsymbol{n}}}} = \left(\boldsymbol{K}_1\frac{\boldsymbol{a}^3_{\mathrm{H^+}}}{\boldsymbol{a}_{\mathrm{Al^{3+}}}}\right)^{1/\boldsymbol{n}} \tag{3}$$

Within the context of Transition State Theory (e.g. Eyring, 1935; Lasaga, 1981; Aagaard and Helgeson, 1982; Gin et al., 2008), the forward or far-from-equilibrium dissolution rate, $\boldsymbol{r}_+$, is proportional to the concentration of these partially detached Si near the surface such that (c.f. Oelkers et al., 1994; Schott and Oelkers, 1995; Schott et al., 2009):

$$\boldsymbol{r}_+ = \boldsymbol{k}_+\boldsymbol{X}_{>\mathrm{Si–O–H_{3/\boldsymbol{n}}}} = \boldsymbol{k}'_+\left(\frac{\boldsymbol{a}^3_{\mathrm{H^+}}}{\boldsymbol{a}_{\mathrm{Al^{3+}}}}\right)^{1/\boldsymbol{n}} \tag{4}$$

where $\boldsymbol{k}_+$ refers to a rate constant and $= \boldsymbol{k}'_+ = \boldsymbol{k}_+\boldsymbol{K}_1^{1/\boldsymbol{n}}$. This approach contrasts to that of Hellmann et al. (2003, 2012), Putnis (2009), Geisler et al. (2010), and Ruiz-Agudo et al. (2012) who argued that leached layers are formed on the surfaces of dissolving multi-oxide minerals and glasses during their dissolution through an interfacial dissolution-precipitation mechanism.

The variation of rate constants with temperature is commonly described by an Arrhenius equation such as (Arrhenius, 1889):

$$\boldsymbol{k}'_+ = \boldsymbol{A}\boldsymbol{e}^{-\left(\frac{\boldsymbol{E_A}}{\boldsymbol{RT}}\right)} \tag{5}$$

where $\boldsymbol{A}$ stands for a pre-exponential constant, $\boldsymbol{E_A}$ designates the activation energy, $\boldsymbol{R}$ refers to the gas constant, and $\boldsymbol{T}$ signifies the absolute temperature. Combining Eqs.

(4) and (5) gives an equation describing natural glass forward dissolution rates with respect to the temperature and aqueous solution composition:

$$r_+ = Ae^{-\left(\frac{E_A}{RT}\right)}\left(\frac{a^3_{H^+}}{a_{Al^{3+}}}\right)^{1/n} \quad (6)$$

This equation will be used below to describe the measured dissolution rates of rhyolitic glass.

3. SAMPLE PREPARATION AND EXPERIMENTAL METHODS

The rhyolitic glass used in the experiments was collected from volcanic ash originally deposited during the 1362 eruption of the Öraefajökull, in south-eastern Iceland. The glass contains less than 1% quenched crystals. The chemical composition of the sample is given in Table 1, and is equivalent to $Na_{0.14}K_{0.06}Ca_{0.01}Fe_{0.04}Al_{0.21}SiO_{2.50}$. The glass was ground and sieved to obtain the 125–250 μm size fraction. This fraction was cleaned ultrasonically using first deionized water, then acetone to remove fine particles. The glass was then dried overnight at 110 °C. The surface area, as determined using a Quantachrome Autosorb-1 using N_2 gas, was 4300 ± 10% $cm^2\ g^{-1}$. The geometric surface area of this powder, estimated assuming that the glass powder is comprised of identical 187.5 μm cubes, is 324 $cm^2\ g^{-1}$ (c.f. Wolff-Boenisch et al., 2011). Glass powders were analyzed before and after disso-

Table 1
Composition of the rhyolitic glass used in the present study and those considered in Fig. 9.*

Study	SiO_2	TiO_2	Al_2O_3	Fe_2O_3	FeO	MnO	MgO	CaO	Na_2O	K_2O	P_2O_5
This study (rhyolite)	70.60	0.24	13.00	2.40	1.18	0.10	0.02	0.97	5.45	3.41	0.02
White (1983)	74.23	–	11.28	0.43	0.25	–	0.2	0.41	–	4.66	–
Kharkansis et al. (1980)	74.9	0.04	14.2	0.29	0.49	0.03	0.02	0.53	4.68	4.59	–
Malow and Ewing (1981)	76[a]	–	–	–	–	–	–	–	–	–	–
Techer (1999)	73.9	–	13.7	–	1.71	–	0.02	0.79	4.2	5.66	–
Berger et al. (1994)	45.6	–	14.5	–	9.8	–	4].1	8.7	3.6	–	–
Crovisier et al. (1985)	45.4	2.53	17.4	–	10.0	0.21	3.4	9.04	4.87	4.04	–
Guy and Schott (1989)	45.5	–	13.9	–	9.7	–	4.5	8.9	2.8	–	–
Daux et al. (1997)	47.67	1.71	14.37	–	10.1	–	7.57	10.73	2.56	0.2	0.18
Gislason and Eugster (1987)	48.1	1.6	14.6	10.9	–	0.2	Q11	11.8	2	0.3	0.2
Techer (1999)	49.34	1.77	14.79	10.85	–	0.19	7.89	10.85	2.67	0.19	0.1

* Composition given in oxide %.
[a] Only SiO_2 data provided in the study.

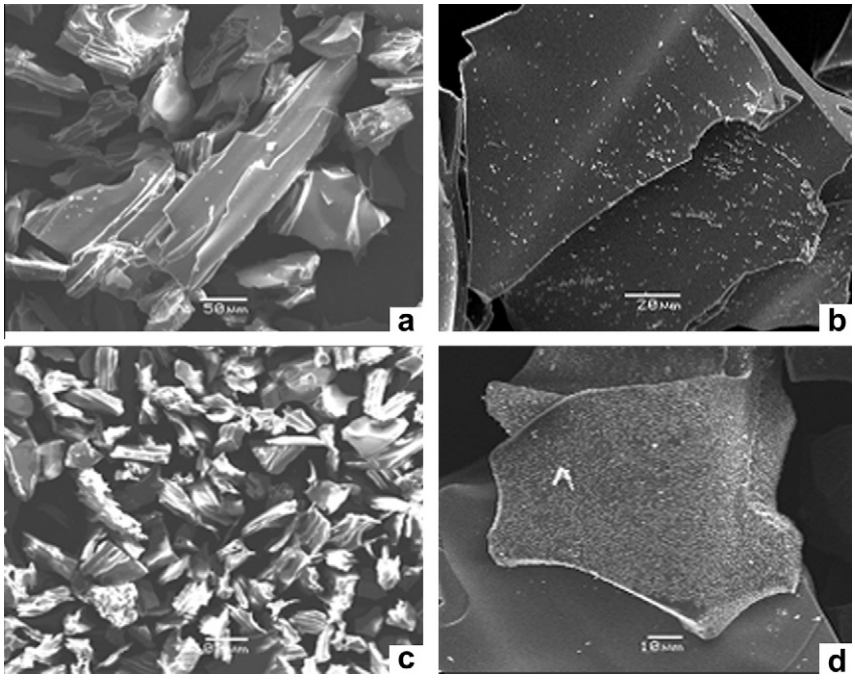

Fig. 1. SEM images of the rhyolite glass powder. Images a and c show the glass before dissolution experiments Images b and d show glass powder after it had been dissolved during experimental series M. The initial rhyolitic glass grains powder is free of fine particles, and appears to have sharp edges. The reacted glass exhibits rounded edges, and the presence of some secondary precipitation.

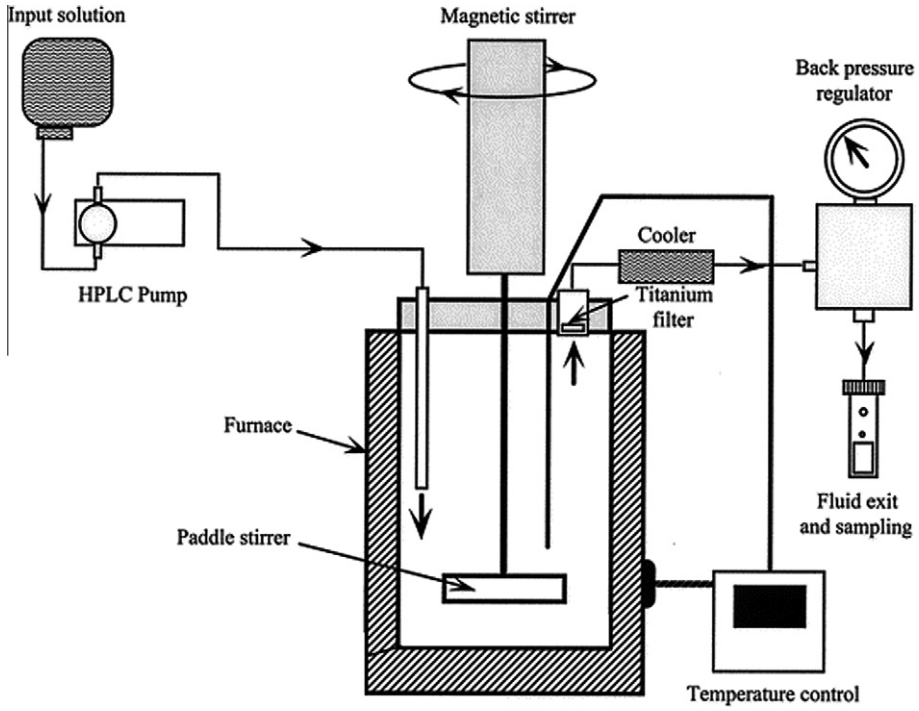

Fig. 2. Diagram of the reactor system used in the dissolution experiments, modified from Gauthier et al. (1994) – see text.

lution experiments using a LEO 435 VP Scanning Electron Microscope (SEM). SEM images of the glass powder before experiments are shown in Figs. 1a and c. It can be seen in this figure that the initial rhyolitic glass grains are free of fine particles, and appear to have sharp edges.

All dissolution experiments were performed in titanium mixed-flow reactor systems such as illustrated in Fig. 2. Application of mixed-flow reactors to measure mineral dissolution rates have been described in detail by Dove and Crerar (1990), Berger et al. (1994), and Oelkers and Schott (1995, 1999). A High Precision/High Pressure Liquid Chromatography (HPLC) pump provided continuous fluid flow ranging from 0.1 to 7 g/min during the experiments. The precision of the fluid flow rates was ±4%. The volume of the titanium reactor was 300 mL. The solution within the reactor was stirred by a Parr magnetically driven stirrer, the temperature controlled by a Parr controlled furnace, and elevated pressure was maintained using a back pressure regulator. The temperature of individual experiments ranged from 40 to 200 °C, and pressure for experiments performed at >100 °C was kept slightly above the H_2O liquid–vapour curve. The fluid left the reactor through a 2 μm titanium filter, quenched, and passed through the back pressure regulator to the outlet, where it was sampled.

Experiments were performed in series consisting of several experiments performed on a single rhyolitic glass powder. Each experimental series is distinguished by the prefix on the experiment number. For example, series A consists of experiments A-1, A-2, A-3, etc. At the beginning of each experimental series the reactor was dismantled at ambient conditions. A specific mass of dry glass powder was placed in the reactor. The reactor was filled with the initial inlet fluid, closed, and placed in the furnace. The temperature, pressure, fluid flow, and stirring rate were adjusted to desired settings. The fluid flow rate and outlet fluid composition were measured regularly. Steady-state Si concentrations were attained after 3–10 days depending on pH and flow rate. After steady-state was verified with a minimum of three constant Si concentrations in the outlet fluid samples obtained over several residence times[1], the inlet fluid composition, and/or fluid flow rate were changed to the next desired experimental condition.

The inlet fluids used in this study comprised demineralised H_2O plus sufficient quantities of reagent grade HCl, NH_4Cl, and/or NH_3 to obtain a 0.01 mol/kg ionic strength solution of the desired pH at 25 °C. Reagent grade $AlCl_3 \cdot 6H_2O$, $Na_2SiO_3 \cdot 5H_2O$, or oxalic acid were added to some of these solutions to assess the effect of Al, Si, or oxalic acid, respectively on rates. Compositions of all inlet solutions are listed in Table 2.

Each fluid sample was divided before analysis. One part of each fluid sample was used for pH measurement at 25 °C using a 713 Metrohm pH meter coupled to a Mettler Toledo Inlab® 422. The other part of the fluid samples was acidified with concentrated suprapure HNO_3 before Al and Si analysis. The aqueous silica concentration of all inlet and outlet fluids were measured using the molybdate blue method of Fishman and Friedman (1989) with a Varyan Spectrophotometer using 1 and 5 cm flow cells. All standards and blanks were obtained using the experimental inlet solutions as diluents. The precision of the aqueous Si concentra-

[1] The residence time is defined as the volume of the reactor divided by the reactive fluid flow rate.

Table 2
Composition of all solutions used in the experiments.

Experiment	HCl (mol/L)	NH_4Cl (mol/L)	NH_4OH (mol/L)
A-*n*	0.01	–	–
B-*n*	0.001	0.009	–
C-1	0.001	0.009	–
C-2	–	0.0014	0.0088
C-3	–	0.0015	0.0085
D-1	–	0.004	0.0085
E-1	–	0.004	0.0035
F-n	0.01	–	–
G-1	0.01	–	–
H-*n*	0.01	–	–
I-1	0.00001	0.00999	–
J-1	–	0.00999	0.00001
K-1	0.01	–	–
K-2	0.001	0.009	–
K-3	0.0001	0.009	–
L-1	0.01	–	–
L-2	0.001	0.09	–
L-3-4	0.001	0.009	–
L-5	0.0001	0.0099	–
L-6-7-8-9-10-11-12	0.01	–	–
M-1	0.001	0.09	–
M-2-3	0.001	0.009	–
M-5	0.0001	0.0099	–

The Al, Si and oxalic acid were added to these solutions in the concentrations as specified in Table 2. *n* indicates that the whole series as the same input solution composition.

tion measurements was within 3% for concentrations above 0.5 mg/kg Si, but close to 10% at lower concentrations.[2] The aluminum concentration was determined by atomic absorption at the Lara-Europe Analyses laboratory in Toulouse, the catechol violet method of Dougan and Wilson (1974), and by atomic adsorption at the GET in Toulouse using a Perkin Elmer Zeeman 5000. The consistency been between analytical methods was better than ±10%.

4. EXPERIMENTAL RESULTS

For each input fluid composition and flow rate, the reaction was allowed to proceed until the output fluid composition attained a steady-state. Steady-state fluid compositions were used to calculate rhyolitic glass dissolution rates using:

$$\boldsymbol{r}_{+,i} = \left(\frac{\boldsymbol{q}\Delta \boldsymbol{c}_i}{\boldsymbol{S}\boldsymbol{m}\nu_i}\right) \tag{7}$$

where $\boldsymbol{q}$ designates the fluid flow rate, $\Delta \boldsymbol{c}_i$ refers to the change in concentration between the inlet and outlet fluid of the subscripted element, $\boldsymbol{S}$ denotes the specific surface of the glass, $\boldsymbol{m}$ represents the mass of glass in the reactor, and ν_i signifies the stoichiometric number of moles of the *i*th element in the glass formula normalised to one mole of silica. The surface area used in this calculation was the BET surface area of the initial rhyolitic glass powder. Input and output fluid compositions, flow rates, computed steady-state dissolution rates and saturation indices with respect to diaspore for all experiments are listed in Tables 2 and 3.

The stoichiometry of these dissolution experiments at steady-state can be assessed with the aid of Fig. 3, where dissolution rates calculated from the outlet fluid Al concentrations, are plotted against corresponding dissolution rates calculated from the outlet fluid Si concentrations. Rates based on Al release tend to be lower than those calculated from Si release in those experiments performed in fluids that were supersaturated with respect to diaspore. The possibility that a secondary phase precipitates in some of these experiments is confirmed by post-experiment SEM images such as shown in Fig. 1b and d. All other experiments exhibit close to stoichiometric Al versus Si release.

The variation of measured steady-state rhyolite glass dissolution rates as a function of outlet fluid Al, Si, and oxalic acid concentration at 80 °C and pH 2 is shown in Fig. 4. Significant scatter is apparent in these diagrams. Nevertheless, rates appear to decrease with increasing Al concentrations. In addition, all rates measured in the presence of aqueous oxalate are higher than those measured in oxalate-free fluids. Rates exhibit a scattered distribution as a function of reactive fluid Si concentration. The degree to which this observed rate behaviour, as well as those of other rates measured at 80 °C are consistent with Eq. (4) can be assessed with the aid of Fig. 5 where the logarithm of measured steady-state dissolution rates of rhyolitic glass is plotted as a function of $\log(\boldsymbol{a}^3_{H^+}/\boldsymbol{a}_{Al^{3+}})$. As seen in this figure all steady-state rates measured at this temperature and pH are consistent with Eq. (4) and $\boldsymbol{n} = 11.1 \pm 2$. The uncertainty on $\boldsymbol{n}$ was estimated from the distribution of data in Fig. 5.

The variation of measured steady-state rhyolite glass dissolution rates as a function of outlet fluid pH at 80 °C is shown in Fig. 6. Rates exhibit a typical behaviour as a function of pH. Rates tend to decrease with increasing pH at acid conditions then increase with increasing pH at basic conditions. This behaviour can be attributed, within the dissolution mechanism described above, to the effect of pH on the aqueous activity ratio $(\boldsymbol{a}^3_{H^+}/\boldsymbol{a}_{Al^{3+}})$ (c.f. Oelkers and Gislason, 2001). It can be seen in Fig. 6 that measured rates exhibit the same overall trend as calculated from Eq. (4) and the parameters obtained from the regression curve shown in Fig. 5.

The variation of measured steady-state rhyolite glass dissolution rates at pH ~ 2 as a function of temperature are quantified in the present study using the empirical Arrhenius equation (Eq. (5)). The activation energy and pre-exponential constant in Eq. (5) were obtained with the aid of the plot shown in Fig. 7. This figure illustrates the logarithm of $\boldsymbol{r}_+(\boldsymbol{a}^3_{H^+}/\boldsymbol{a}_{Al^{3+}})^{-1/11.1}$ plotted as a function of reciprocal temperature. Regression of these data, as illustrated in Fig. 8 yields $\boldsymbol{A} = 1.4 \times 10^{-5}$ mol/cm^2/s and $\boldsymbol{E_A} = 55.15$ kJ/mol. This activation energy is similar to that found for other aluminosilicates glasses and minerals (Crovisier et al., 1985; Grambow et al., 1985; Gislason and Eugster, 1987; Guy and Schott, 1989; Crovisier et al., 1990; Berger et al., 1994; Daux et al., 1997) suggesting a similar dissolution mechanism for these phases.

[2] Uncertainties in analytical precision this study correspond to the standard deviation of repeated analyses. The reported percent corresponds to ratio of the standard deviation to the reported value.

Table 3
Experimental conditions and rhyolitic glass steady-state dissolution rates obtained during the study.

Run	T° (°C)	pH	Mass of powder (g)	Fluid flow rate (g/min)	$C_{Si(inlet)}$ (ppm)	$C_{Al(inlet)}$ (ppm)	$C_{Si(outlet)}$ (ppm)	$C_{Al(outlet)}$ (ppm)	$[Ox]_{inlet}$ (mol/kg)	Log a_{Al}	Log r_+ (mol/cm^2/s) Calculated from:		Diaspore SI	Log r_+ (mol/cm^2/s) predicted
											C_{Si}	C_{Al}		
A-7	200	2.1	2.00	7.0	–	–	32.07	0.55	–	−6.02	−10.81	−11.88	0.49	−10.97
F-1	175	2.1	0.42	2.5	–	–	11.60	1.41	–	−5.19	−11.03	−11.25	0.60	−11.39
A-6	175	2.1	2.00	7.0	–	–	10.36	1.28	–	−5.23	−11.30	−11.51	0.53	−11.38
A-1	150	2.0	2.00	0.1	–	–	24.51	5.21	–	−4.31	−12.77	−12.75	0.22	−11.81
F-2	150	2.1	0.42	2.5	–	–	2.61	0.79	–	−5.13	−11.68	−11.50	−0.34	−11.76
C-1	150	3.2	1.18	7.0	–	–	2.67	0.05	–	−7.40	−11.66	−12.68	0.87	−11.86
A-5	130	2.0	2.00	7.0	–	–	1.51	0.42	–	−5.26	−12.14	−12.00	−1.29	−12.07
B-2	130	3.2	0.99	7.0	–	–	0.82	0.05	–	−6.59	−12.09	−12.59	0.71	−12.26
G-1	120	2.0	0.51	2.5	–	5	0.34	6.33	–	−4.06	−12.63	−10.67	−0.55	−12.35
F-3	120	2.0	0.45	2.6	–	1	0.31	1.56	–	−4.65	−12.61	−11.22	−1.15	−12.30
F-4	120	2.0	0.49	2.6	–	5	0.30	6.42	–	−4.05	−12.66	−10.63	−0.52	−12.36
K-3	120	3.6	0.68	0.5	–	–	1.98	0.08	–	−6.94	−12.70	−13.42	1.42	−12.53
K-1	120	1.9	0.68	0.5	–	–	1.08	0.25	–	−5.46	−12.96	−12.90	−2.25	−12.20
K-2	120	2.9	0.68	0.5	–	–	0.62	0.15	–	−5.85	−13.20	−13.13	0.40	−12.43
A-3	110	2.1	2.00	7.0	–	–	0.47	0.19	–	−5.51	−12.65	−12.34	−2.08	−12.45
B-1	110	3.0	0.99	7.0	–	–	0.36	0.08	–	−6.03	−12.45	−12.44	0.12	−12.64
H-2	80	2.0	1.16	0.5	–	–	0.79	0.37	–	−5.18	−13.33	−12.96	−3.29	−13.09
H-1	80	2.0	1.16	1.0	–	–	0.29	0.25	–	−5.35	−13.46	−12.84	−3.62	−13.06
A-2	80	2.1	2.00	2.0	–	–	0.18	0.08	–	−5.82	−13.62	−13.28	−3.49	−13.05
H-4	80	2.1	1.16	5.0	–	–	0.20	0.04	–	−6.12	−12.93	−12.99	−4.03	−13.03
H-3	80	2.1	1.16	7.0	–	–	0.12	0.04	–	−6.12	−12.98	−12.79	−4.21	−13.01
I-1	80	5.3	0.89	0.5	–	–	0.24	0.00	–	−10.50	−13.74	−14.94	1.09	−13.49
J-1	80	6.2	1.06	0.5	–	–	0.32	0.01	–	−13.34	−13.69	−14.49	1.30	−13.49
C-3	80	10.1	1.08	0.5	–	–	0.81	0.25	–	−27.47	−13.28	−13.11	0.10	−13.27
E-1	80	8.8	1.24	0.5	–	–	0.34	0.03	–	−23.17	−13.73	−14.14	0.41	−13.30
D-1	80	9.8	1.02	0.5	–	–	0.65	0.15	–	−26.48	−13.36	−13.31	0.21	−13.26
L-1	80	2.0	1.47	1.0	–	–	0.87	0.21	–	−5.43	−13.09	−13.02	−3.54	−13.07
L-2	80	2.4	1.47	1.0	–	0.8	0.52	1.10	–	−4.63	−13.30	−12.85	−1.80	−13.23
L-3	80	2.0	1.47	1.0	–	10.8	0.32	11.06	–	−3.75	−13.53	−12.94	−1.84	−13.22
L-4	80	2.0	1.47	1.0	–	100.0	0.33	100.54	–	−2.98	−13.53	−12.62	−1.05	−13.29
L-5	80	1.9	1.47	0.9	–	50.0	0.31	50.20	–	−3.18	−13.57	−13.06	−1.69	−13.23
L-6	80	2.0	1.47	1.0	–	–	0.77	0.19	–	−5.47	−13.14	−13.06	−3.65	−13.06
L-7	80	2.0	1.47	0.8	1.1	–	2.22	0.20	–	−5.45	−13.07	−13.12	−3.62	−13.06
L-8	80	2.0	1.47	1.0	10.2	–	10.49	0.17	–	−5.49	−13.52	−13.11	−3.70	−13.06
L-9	80	2.1	1.47	1.0	–	–	0.67	0.15	–	−5.48	−13.21	−13.17	−3.69	−13.07
M-1	80	2.5	0.60	2.5	–	–	0.08	0.02	–	−6.35	−13.36	−13.24	−3.11	−13.11
M-2	80	3.0	0.60	2.5	–	–	0.05	0.02	–	−6.35	−13.58	−13.19	−1.41	−13.25
M-3	80	3.0	0.61	2.5	–	–	0.04	0.02	–	−6.36	−13.62	−13.25	−1.46	−13.25
M-4	80	3.1	0.60	2.5	–	–	0.07	0.01	–	−7.35	−13.40	−13.47	−1.44	−13.18
M-5	80	4.1	0.60	2.5	–	–	0.04	0.00	–	−3.68	−13.64	−14.06	−1.79	−13.78
L-10	80	2.1	1.47	1.0	–	–	1.83	0.52	0.0100	−5.01	−12.79	−12.64	−2.93	−13.13
L-11	80	2.1	1.47	1.0	–	–	1.81	0.47	0.0010	−5.05	−12.76	−12.65	−2.96	−13.12
L-12	80	2.1	1.47	1.0	–	–	1.66	0.44	0.0001	−5.08	−12.79	−12.68	−3.13	−13.11
A-4	40	2.1	2.00	7.0	–	–	0.05	0.01	–	−6.69	−13.61	−13.62	−6.83	−14.01

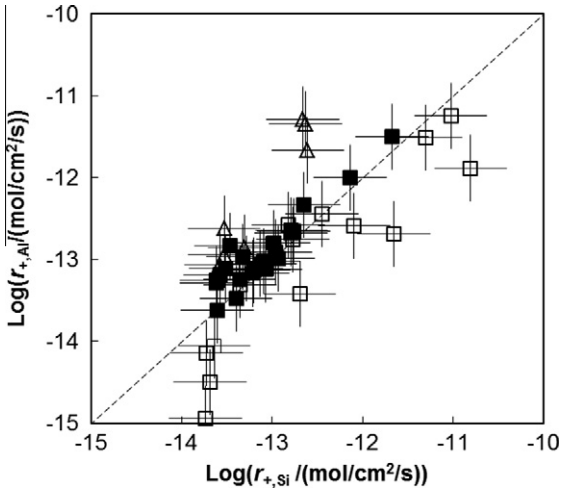

Fig. 3. Logarithmic plot of steady-state forward rhyolitic glass dissolution rates determined from the difference in the inlet and steady-state outlet fluid Al concentration plotted as a function of the corresponding rate calculated from change in Si concentration using Eq. (7). Rates obtained for experiments for which the outlet fluid was supersaturated with respect to diaspore are depicted by open squares, rates obtained from Si-rich inlet fluids are depicted by open triangles and all other rates are depicted by solid squares. The solid line in this figure corresponds to equal Al versus Si rates. The error bars in this figure correspond to a ±0.3 log unit uncertainty in computed rates.

The distribution of points shown in Figs. 4, 6 and 7 leaves little doubt that rhyolite glass steady-state dissolution rates can be described as a function of temperature and fluid composition using Eq. (6). Consistent with the regression curves described above steady-state forward rhyolite glass dissolution rates are consistent with

$$r_+ = (1.4 \times 10^{-5}\ \text{mol/cm}^2/\text{s}) e^{-\left(\frac{55.15\ \text{kJ/mol}}{RT}\right)} \left(\frac{a^3_{H^+}}{a_{Al^{3+}}}\right)^{1/11.1} \quad (8)$$

The degree to which Eq. (8) describes the rate obtained in the present study can be assessed with Fig. 8. Overall 35 of the 43 measured rates are within ±0.4 log units of those calculated using Eq. (8).

5. EXPERIMENTAL UNCERTAINTIES

Uncertainties associated with the rates generated in this study arise from a variety of sources, including the measurement of aqueous solution concentrations, fluid flow rates, and glass surface areas. The uncertainties in the measured values of the total aqueous silica and aluminium concentration are on the order of ±10% or less. Computational and experimental uncertainties on the pH measured are on the order of ±0.04 pH units. Uncertainties in fluid flow rate measurements are not more than 4%. In contrast uncertainties associated with the measurement of the surface area of the initial rhyolitic glass powder is ±10%. If uncertainties were estimated exclusively from the sum of these contributions, an overall uncertainty of the dissolution rates reported in this would be on the order of 20%. Nevertheless some additional uncertainty may arise due to changes in glass reactive surface area during the experiments. Accord-

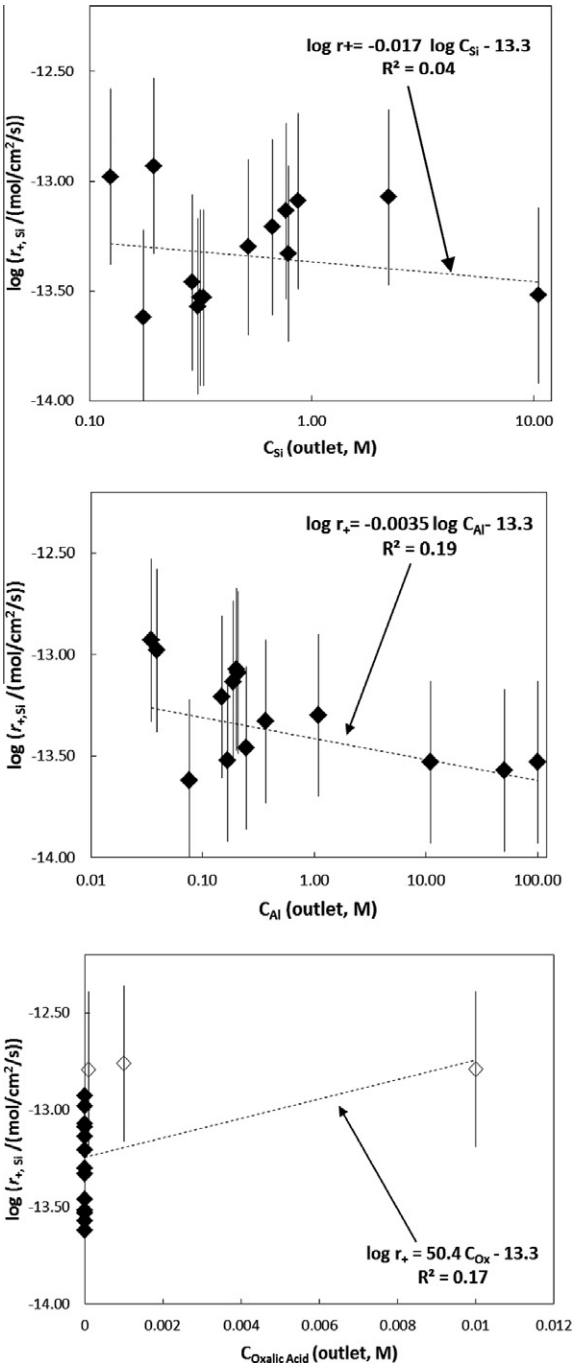

Fig. 4. Measured steady-state rhyolitic glass dissolution rates obtained at 80 °C and pH of 2 as a function of the outlet fluid aqueous (a) Al, (b) Si, and (c) oxalic acid concentration. The symbols correspond to measured rates and the dashed curves represent linear least squares fits of the data in each plot. The equation for each fit and their associated coefficient of determination (R^2) are provided in each plot. The error bars in this figure correspond to a ±0.3 log unit uncertainty in computed rates.

ing to mass balance calculations, less than 5% of the initial rhyolitic glass powder was dissolved in any experimental series other than series A where nearly 15% was dissolved. As emphasized by Gauthier et al. (1994), the degree to which reactive surface area varies in response to dissolution

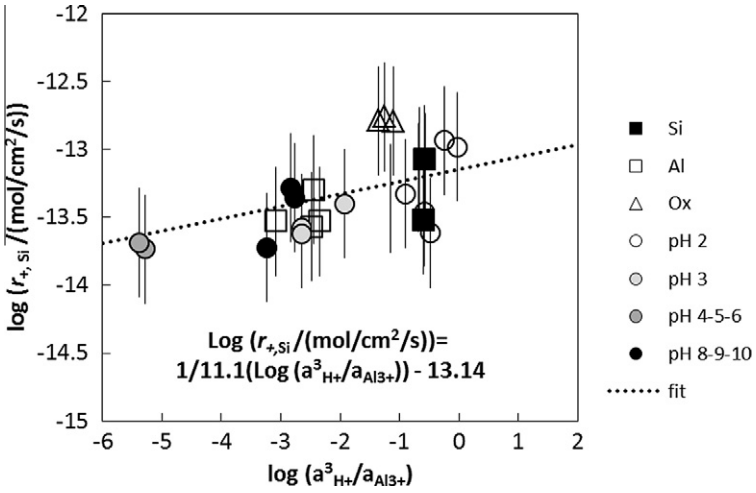

Fig. 5. Logarithmic plot of measured steady-state rhyolite glass dissolution rates based on Si release as a function of $(a^3_{H^+}/a_{Al^{3+}})$. The open triangles, open squares, and filled squares correspond to rates measures in oxalic acid bearing inlet fluids, Al-rich inlet fluids and Si-rich inlet fluids, respectively. The line in this figure is consistent with Eq. (4) and $n = 11.1$. The error bars in this figure correspond to a ±0.3 log unit uncertainty in computed rates.

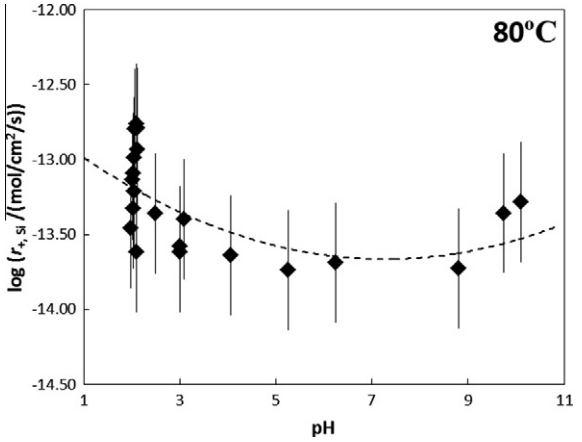

Fig. 6. The logarithm of measured steady-state rhyolitic glass dissolution rates plotted as a function of pH. The symbols correspond to measured rates based on Si release, whereas the dashed curve was calculated using Eq. (3), $n = 11.1$ and $k'_+ = 10^{-13.14}$ mol/cm²/s for a reactive fluid containing a total dissolved Al concentration of 10^{-5} mol/kg. Aqueous Al activities required to compute the dashed curve were calculated using PHREEQC assuming only the only aqueous Al complexes present were $AlOH^{2+}$, $Al(OH)^+_2$, $Al(OH)^0_3$, and $Al(OH)^-_4$. The error bars in this figure correspond to a ±0.3 log unit uncertainty in computed rates.

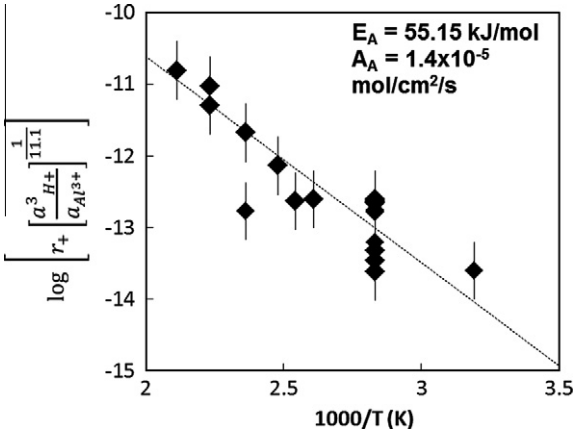

Fig. 7. Logarithm of $r_+(\frac{a^3_{H^+}}{a_{Al^{3+}}})^{-1/11.1}$ plotted as a function of reciprocal temperature. Symbols correspond to measured steady state rhyolitic glass dissolution rates whereas the dashed line is consistent with Eq. (6), $A = 1.4 \times 10^{-5}$ mol/cm²/s and $E_A = 55.15$ kJ/mol. The error bars in this figure correspond to a ±0.3 log unit uncertainty in computed rates.

is currently impossible to define unambiguously. Consideration of the scatter in the Figs. 3–7 suggests that the overall uncertainty on the rhyolitic glass dissolution rates measured in the present study to be on the order of ±0.3 log units.

6. DISCUSSION

6.1. Comparison with previous glass dissolution rates

The temperature variation of pH 2 rhyolitic and basaltic glass dissolution rates is shown in Fig. 9. A least squares fit of the basaltic glass steady-state dissolution rates obtained from the literature suggests an apparent activation energy of 66.6 kJ/mol with 95% confidence limits of ±20.53 kJ/mol. This apparent activation energy is close to that obtained for rhyolite glass in the present study. This coherence supports the likelihood that these two glasses share the same dissolution mechanism and the rate limiting step for the dissolution of both of these glasses is the breaking of Si–O bonds in the Al–O–Si glass framework.

It is curious, however, that a least squares fit of temperature dependence of the available steady-state rhyolitic glass steady-state dissolution rates yields an apparent activation energy of just 42.79 kJ/mol with 95% confidence limits of ±28.2 kJ/mol. The difference between the activation energies reported above and those generated from the data

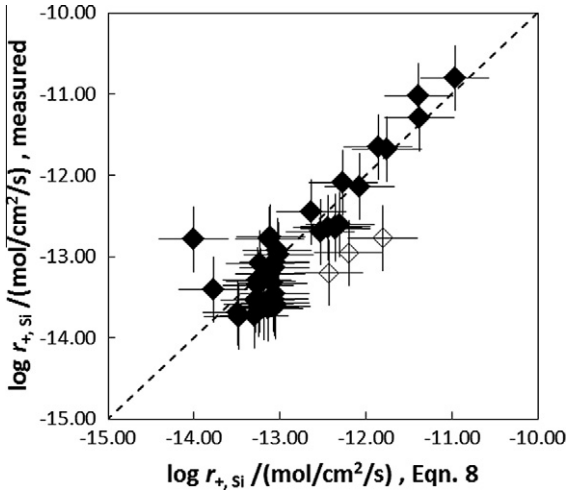

Fig. 8. The logarithm of measured steady-state rhyolitic glass dissolution rates plotted as a function of corresponding rates calculated using Eq. (6), $n = 11.1$, $A = 1.4 \times 10^{-5}$ mol/cm^2/s and $E_A = 55.15$ kJ/mol. The symbols represent rates, whereas the solid line traces equal values for these two rates – see text.

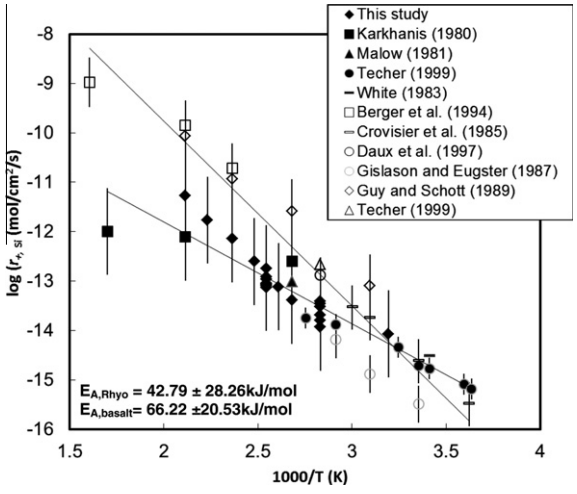

Fig. 9. Comparison of steady-state rhyolitic and basaltic glass forward dissolution rates at pH 2 as a function of reciprocal temperature. The origin of the plotted rates dissolution rates are given in the figure where open and filled symbols correspond to rates of basaltic and rhyolitic glass, respectively, and the chemical formula of each glass is provided in Table 1. Error bars were selected to correspond to that reported in each study. The solid curves correspond to a least squares fit of the two data sets. Apparent activation energies obtained from the slope of these regression curves and their 95% confidence limits are provided in the figure.

shown in Fig. 9 stem from the differing temperature dependence of the Techer (1999) and Kharkansis et al. (1980) data sets which define a smaller dependence on temperature than those generated in this study. A smaller temperature dependence, however, suggests that at pH 2 and temperatures less than ~25 °C rhyolitic glass dissolution rates would be faster than those of basaltic glass, which is inconsistent with the systematic variation of the dissolution rates of these at 25 °C reported by Wolff-Boenisch et al. (2004a). Nevertheless, despite these ambiguities, pH 2 apparent activation energies of rhyolite and basaltic glass are identical within the 95% confidence limits of the regression analysis. Equal apparent activation energies would imply that the ratio between rhyolitic and basaltic glass dissolution rates would be independent of temperature.

6.2. The significance of *n*

One distinct feature of rhyolitic glass dissolution rates is that they are consistent with a higher value of ***n*** compared to that of basaltic glass. This difference relates to how aqueous Al and pH effects dissolution rates. The regressed value of ***n*** generated above for rhyolite glass dissolution is 11.1 whereas that for basaltic glass is 3 (Oelkers and Gislason, 2001). Thus the effect of pH change on the logarithm of the dissolution rates of basaltic glass will be roughly 3.5 times that of the corresponding change on rhyolite glass. Similarly the effect of a change in aqueous Al activity, and thus the concentration of Al complexing agent such as organic ligands will be significantly lower on rhyolite glass than basaltic glass.

It is of interest to note that within the dissolution mechanism, ***n*** stands for the stoichiometric number of activated complexes one obtains from the removal of one Al atom from the near surface. The values of ***n*** for rhyolite glass obtained in this study and those reported in the literature (e.g. Wolff-Boenisch et al., 2004a) are higher than those for basaltic glass. This suggests that as the Al content of the glass decreases, more Si-rich activated complexes are formed by the removal of each Al.

6.3. Significance of measured rates on natural processes

One distinct feature of the dissolution of natural glasses as opposed to that of minerals is that they rarely approach equilibrium with natural fluids. As such measured far-from-equilibrium glass dissolution rates determined in laboratory studies may be more directly applicable to natural systems. A critical aspect of natural weathering is the ability of organisms to obtain essential nutrients from rocks and soils. Many organisms obtain nutrients by secreting organic ligands to accelerate dissolution rates (e.g. Hilgard, 1914; Huang and Keller, 1972; Powel et al., 1980; Ludwig et al., 1995). The relatively small effect of changing aqueous Al activity on rhyolite glass dissolution rates suggests that microbial enhancement of the dissolution of this glass by organic ligand secretion will be limited compared to other Al-silicates such as plagioclase and basaltic glass. This conclusion is consistent with the relative poor productivity of felsic volcanic rocks (e.g. Heckkman and Rasmussen, 2011).

7. CONCLUSION

The variation of steady-state rhyolite glass dissolution rates with reactive fluid composition presented above suggests that its dissolution is limited by the relatively slow liberation of Si tetrahedra after their partial liberation via Al

for proton exchange reactions. This rate behaviour is exhibited by all natural aluminosilicate glasses (c.f. Wolff-Boenisch et al., 2004a). The conclusion that volcanic glasses proceed by an identical mechanism is supported by their similar activation energies. Measured rhyolitic glass dissolution rates are, however, one to two orders of magnitude slower than those of basaltic glass, demonstrating an increased resistance to dissolution with a decreasing Al content in the glass structure. As the activation energy of rhyolite glass is likely similar to that of basaltic glass, the relative difference in the dissolution rates of these two glasses will remain near constant with increasing temperature.

The systematic behaviour of rhyolite dissolution rates as a function of temperature, pH, and aqueous fluid composition allowed the generation of a simple equation to describe measured rates. The success of this equation to accurately describe rates over wide ranges of temperature and fluid composition, including those containing aqueous organic ligands suggests this rate equation can provide useful estimates of rhyolite glass dissolution rates in a variety of natural systems.

ACKNOWLEDGEMENTS

We would like to thank Alain Castillo and Jean-Claude Harrichoury for technical assistance throughout the duration of the experimental work, Carole Causserand for her generous help during the analytical part of the work, and Philippe de Parseval for aid creating SEM images. Three reviewers provided sets of enlightened comments leading to significant improvements to this contribution. We are also grateful to Domenick Wolff-Boenisch for providing the rhyolite glass used in this study. We thank Per Aagaard, Stacey Callahan, Oleg Pokrovsky, Jacques Schott, Pascale Bénézeth, Domenick Wolff-Boenisch and Morgan T. Jones for helpful discussions during the course of this study. Support from Centre National de la Recherche Scientifique, and the European Community through the MIN-GRO Research and Training Network (MRTN-CT-2006-035488) is gratefully acknowledged.

REFERENCES

Aagaard P. and Helgeson H. C. (1982) Thermodynamic and kinetic constraints on reaction-rates among minerals and aqueous solutions: I. Theoretical considerations. *Am. J. Sci.* **282**, 237–285.

Allnatt A. R., Bancroft G. M., Fyfe W. S., Jacobs P. W. M., Karkhanis S. N., Melling P. J., Nishijima A., Vempati C. S. and Tait J. (1983) Leaching behaviour and electrical conductivity of natural rhyolite and modified synthetic rhyolites. *Chem. Geol.* **38**, 329–357.

Arsouze T., Dutay J.-C., Lacan F. and Jeandel C. (2009) Reconstructing the Nd oceanic cycle using a coupled dynamical-biogeochemical model. *Biogeosciences* **6**, 1–18.

Arrhenius S. (1889) Über die Reaktionsgeschwindigkeit bei der Inversion von Rohzucker durch Säuren. *Z. Phys. Chem.* **4**, 226–248.

Berner R. A., Lasaga A. C. and Garrels R. M. (1983) The carbonate-silicate geochemical cycle and its effect on atmospheric carbon-dioxide over the past 100 million years. *Am. J. Sci.* **283**, 641–683.

Berger G., Schott J. and Loubet M. (1987) Fundamental processes controlling the 1st stage of alteration of a basalt glass by seawater – an experimental study between 200 and 320 °C. *Chem. Geol.* **71**, 297–312.

Berger G., Schott J. and Guy C. (1994) Dissolution rate of basaltic glass in silica-rich solutions: implications for the long-term alteration. *Geochim. Cosmochim. Acta* **22**, 4875–4886.

Brady J. P. and Gislason S. R. (1997) Seafloor weathering controls on atmospheric CO_2 and global climate. *Geochim. Cosmochim. Acta* **61**, 965–973.

Cailleteau C., Angeil F., Deveux F., Gin S., Jestin J., Jollivet P. and Spalla O. (2008) Insight into silicate-glass corrosion mechanisms. *Nat. Mater.* **7**, 978–983.

Carey S. N. (1997) Influence of convective sedimentation on the formation of widespread tephra layers in deep sea. *Geology* **25**, 839–842.

Chester D. K., Degg M., Duncan A. M. and Guest J. E. (2000) The increasing exposure of cities to the effects of volcanic eruptions: a global survey. *Global Environ. Change Part B: Environ. Hazards* **2**, 89–103.

Conradt R. (2008) Chemical durability of oxide glasses in aqueous solutions: a review. *J. Am. Ceram. Soc.* **91**, 728–735.

Crovisier J. L., Atassi H., Daux V. and Eberhart J. P. (1990) Hydrolyse d'un verre basaltique tholéitique à 60 °C, dissolution sélective puis congruente par élévation du pH. *C. R. l'Academie. Sci., Ser. II* **310**, 941–952.

Crovisier J. L., Fritz B., Granbow B. and Eberhart J. P. (1985) Dissolution of basaltic glass in seawater: mecanism and rate. *Geochim. Cosmochim. Acta* **51**, 2977–2990.

Crovisier J. L., Honnorez J., Fritz B. and Petit J. C. (1992) Dissolution of subglacial volcanic glasses from Iceland – laboratory study and modeling. *Appl. Geochem.* **7**, 55–81.

Crovisier J. L., Advocat T. and Dussossoy J. L. (2003) Nature and role of natural alteration gels formed on the surface of ancient volcanic glasses (Natural analogues of waste containment glasses). *J. Nucl. Mater.* **321**, 91–109.

Curti E., Crovisier J. L., Morvan G. and Karpoff A. M. (2006) Long-term corrosion behavior of two nuclear waste glasses (MW and SON68): a kinetic and mineral alteration study. *Appl. Geochem.* **21**, 1152–1168.

Daux V., Guy C., Advocat T., Crovisier J. L. and Stille P. (1997) Kinetic aspects of basaltic glass dissolution at 90 °C: role of aqueous silicon and aluminium. *Chem. Geol.* **142**, 109–126.

Dessert C., Dupré B., François L. M., Schott J., Gaillardet J., Chakrapani G. and Bajpai S. (2001) Erosion of Deccan Traps determined by river geochemistry. Impact on global climate and 87Sr/86Sr ratio of seawater. *Earth Planet. Sci. Lett.* **188**, 459–474.

Dickin A. P. (1981) Hydrothermal leaching of rhyolite glass in the environment has implication for nuclear waste disposal. *Nature* **294**, 342–347.

Dougan W. K. and Wilson A. C. (1974) The absorptiometric determination of aluminium in water. A comparison of some chromogenic reagents and the development of an improved method. *Analyst* **99**, 413–430.

Dove P. M. and Crerar D. A. (1990) Kinetics of quartz dissolution in electrolyte solutions using a hydrothermal mixed flow reactor. *Geochim. Cosmochim. Acta* **54**, 955–969.

Dran J.-C., Petit J.-C. and Brousse C. (1986) Mechanism of aqueous dissolution of silicate glasses yielded by fission tracks. *Nature* **319**, 485–487.

Dran J. C., Mea G. D., Paccagnella A. and Petit J. C. (1988) Aqueous dissolution of alkali-silicate glasses: reappraisal of mechanisms by H and Na depth profiling with high energy ion beams. *Phys. Chem. Glasses* **29**, 249–255.

Durant A. J., Bonadonna C. and Horwell C. J. (2010) Atmospheric and environmental impact of volcanic particulates. *Elements* **6**, 235–240.

Eyring H. (1935) The activated complex in chemical reactions. *J. Chem. Phys.* **3**, 107–115.

Fiore S., Huerta F. J., Tazaki K., Huertas F. and Linares J. (1999) A low temperature experimental alteration of a rhyolitic obsidian. *Eur. J. Mineral.* **11**, 455–469.

Fishman M.J. and Friedman L.C. (1989) Methods for determination of inorganic substances in water and fluvial sediments. In *U.S. Geological survey Techniques of Water-Resources Investigation*, Book 5. USGS, Reston, VA, USA, pp. 545.

Flaathen T. K. and Gislason S. R. (2007) The effect of volcanic eruptions on the chemistry of surface waters: the 1991 and 2000 eruptiosn of Mt. Hekla, Iceland. *J. Volcanol. Geotherm. Res.* **164**, 293–316.

Flaathen T. K., Gislason S. R. and Oelkers E. H. (2010) The effect of aqueous sulphate on basaltic glass dissolution rates. *Chem. Geol.* **277**, 345–354.

Gauthier J. M., Oelkers E. H. and Schott J. (1994) Experimental study of K-Feldspar dissolution rate as a function of chemical affinity at 150 °C and pH 9. *Geochim. Cosmochim. Acta* **58**, 4549–4560.

Geisler T., Janssen A., Scheiter D., Stephan T., Berndt J. and Putnis A. (2010) Aqueous corrosion of borosilicate glass under acid conditions: a new corrosion mechanism. *J. Non-Crystal. Mater.* **356**, 1458–1465.

Gin S. and Mestre J. P. (2001) SON 68 nuclear glass alteration kinetics between pH 7 and pH 11.5. *J. Nucl. Mater.* **295**, 83–96.

Gin S., Jegou C., Frugier P. and Minet Y. (2008) Theoretical consideration on the application of the Aagaard–Helgeson rate law to the dissolution of silicate minerals and glasses. *Chem. Geol.* **255**, 14–24.

Gislason S. R. and Eugster H. P. (1987) Meteoric water–basalt interactions. II: a field study in N.E. Iceland. *Geochim. Cosmochim. Acta* **51**, 2827–2855.

Gislason S. R. and Oelkers E. H. (2003) The mechanism, rate and consequence of basaltic glass dissolution: II. An experimental study of the dissolution rates of basalts as a function of pH at temperatures from 6 °C to 150 °C. *Geochim. Cosmochim. Acta* **67**, 3817–3832.

Gislason S. R., Arnórsson S. and Armannsson H. (1996) Chemical weathering of basalt in SW Iceland: effects of runoff, age of rocks, and vegetative/glacial cover. *Am. J. Sci.* **296**, 837–907.

Gislason S. R., Oelkers E. H. and Snorrason Á. (2006) The role of river suspended material in the global carbon cycle. *Geology* **34**, 49–52.

Gislason S. R., Oelkers E. H., Eiriksdottir E. S., Kardjilov M. I., Gisladottir G., Sigfusson G., Snorrason A., Elefsen S., Hardardottir J., Torssander P. and Oskarsson N. (2009) Direct evidence of the feedback between climate and weathering. *Earth Planet. Sci. Lett.* **277**, 213–222.

Gislason S. R., Wolff-Boenisch D., Stefansson A., Oelkers E. H., Gunnlaugsson E., Sigurdardottir H., Sigfusson B., Broecker W. S., Matter J. M., Stute M., Axelsson G. and Fridriksson T. (2010) Mineral sequestration of carbon dioxide in basalt: a pre-injection overview of the CarbFix project. *Int. J. Greenhouse Gas Control* **4**, 537–545.

Gout R., Oelkers E. H., Schott J. and Zwick A. (1997) The surface chemistry and structure of acid leached albite: new insights on the dissolution mechanism of the alkali feldspars. *Geochim. Cosmochim. Acta* **61**, 3013–3018.

Gow A. J. and Williamson T. (1971) Volcanic ash in the Antarctic ice sheet and its possible climatic implications. *Earth. Planet. Sci. Lett.* **13**, 210–218.

Grambow B., Jercinovic M.J., Ewing R.C. and Byers C.D. (1985) In *Materials Research Society Conference Proceedings in Scientific Basis for Nuclear Waste Management*, vol. 50. pp. 263.

Guy C. and Schott J. (1989) Multisite surface reaction versus transport control during the hydrolysis of a complex oxide. *Chem. Geol.* **78**, 181–204.

Heckkman K. and Rasmussen C. (2011) Lithological controls on regolith weathering and mass flux in forested ecosystems of the southwestern USA. *Geoderma* **164**, 99–111.

Hellmann R., Penisson J. M., Hervig K. L., Thomassin J. H. and Abrioux M. F. (2003) An EFTEM/HRTEM high resolution study of the near surface of labradorite feldspar altered at acid pH: evidence for interfacial dissolution-reprecipitation. *Phys. Chem. Miner.* **30**, 192–197.

Hellmann R., Wirth R., Daval D., Barnes J. P., Penisson J. M., Tisserand D., Epicier T., Florin B. and Hervig R. L. (2012) Unifying natural and laboratory chemical weathering with interfacial dissolution–reprecipitation: a study based on nanoscale chemistry of fluid–silicate interfaces. *Chem. Geol.* **294–295**, 203–216.

Holland H. D. (1978) *The Chemistry of the Atmosphere and Oceans*. Wiley, New York.

Hilgard E. W. (1914) *Soils: Their Formation, Properties, Compositions and Relations to Climate and Plant Growth in the Humid and Arid Region 19*. McMillan, New York.

Huang W. H. and Keller W. D. (1972) Organic acids as agents of chemical weathering of silicate minerals. *Nature* **239**, 149–151.

Icenhower J. P., McGrail B. P., Shaw W. J., Pierce E. M., Nachimuthu P., Shuh D. K., Rodiguez E. A. and Steele J. L. (2008) Experimentally determined dissolution kinetics of Na-rich borosilicate glass at far from dissolution conditions. Implications for Transition state theory. *Geochim. Cosmochim. Acta* **72**, 2767–2788.

Jeandel C., Peucker-Ehrenbrink B., Jones M. T., Pearce C. R., Oelkers E. H., Godderis Y., Lacan F., Aumont O. and Arsouze T. (2011) Ocean margins: the missing term for oceanic element budgets? *EOS Trans. Am. Geophys. Union* **92**, 217–224.

Jones M. T. and Gislason S. R. (2008) Rapid releases of metal salts and nutrients following the deposition of volcanic ash into aqueous environments. *Geochim. Cosmochim. Acta* **72**, 3661–3680.

Kettler R. M., Wesoloski D. J. and Palmer D. A. (1998) Dissociation constants of oxalic acid in aqueous sodium chloride and sodium trifluoromethanesulfonate media to 175 °C. *J. Chem. Eng. Data* **43**, 337–350.

Kharkansis S. N., Bancroft G. M., Fyfe W. S. and Brown J. D. (1980) Leaching behaviour of rhyolite glass. *Nature* **284**, 435–437.

Kump L. R., Brantley S. L. and Arthur M. A. (2000) Chemical weathering, atmospheric CO_2, and climate. *Ann. Rev. Earth Planet. Sci.* **28**, 611–667.

Lacasse C. and van den Bogaard P. (2002) Enhanced airborne dispersal of silicic tephras during the onset of northern hemisphere glaciation, from 6 to 0 Ma records of explosive volcanism and climate change in subpolar North Atlantic. *Geology* **30**, 623–626.

Larsen G., Newton A. J., Dugmore A. J. and Vilmundardottir E. G. (2001) Geochemistry, dispersal, volumes and chronology of Holocene silicic tephra layers from the Katla volcanic system, Iceland. *J. Quat. Sci.* **16**, 119–132.

Lasaga A. C. (1981) Transition state theory. *Rev. Mineral.* **8**, 135–169.

Louvat P. and Allegre C. J. (1997) Present denudation rates on the island of Réunion determined by river geochemistry: basalt weathering and mass budget between chemical and mechanical erosions. *Geochim. Cosmochim. Acta* **61**, 3645–3669.

Ludwig C., Casey W. H. and Rock P. A. (1995) Prediction of ligand promoted dissolution rates from the reactivities of aqueous complexes. *Nature* **375**, 44–47.

Magonthier M.-C., Petit J.-C. and Dran J.-C. (1992) Rhyolitic glasses as natural analogues of nuclear waste glasses: behaviour of an Icelandic glass upon natural aqueous corrosion. *Appl. Geochem.* **7**, 83–93.

Malow G. and Ewing R. C. (1981) Nuclear waste glasses and volcanic glasses: a comparison of their stabilities. *Sci. Basis Nuclear Waste Mgt.* **1**, 83–93.

Marini L. (2007) *Geological Sequestration of Carbon Dioxide: Thermodynamics, Kinetics and Reaction Path modeling*. Elsevier, Amsterdam, pp. 470.

Mazer J. J. and Walther J. V. (1994) Dissolution kinetics of silica glass as a function of pH between 40 and 85 °C. *J. Non-Crystal. Solids* **170**, 32–45.

McGrail B. P., Ebert W. L., Bakel A. J. and Peeler D. K. (1997) Measurement of kinetic rate law parameters on a Na–Ca–Al borosilicate glass for low-activity waste. *J. Nucl. Mater.* **249**, 175–189.

McGrail B. P., Schaef H. T., Ho A. M., Chien Yi.-Ju., Dooley J. J. and Davidson C. L. (2006) Potential for carbon dioxide sequestration in flood basalts. *JGR Res.* **111**, B12201. http://dx.doi.org/10.1029/2005JB004169.

Morgan N. A. and Spera F. J. (2001) Glass transition, structural relaxation, and theories of viscosity. A molecular dynamics study of amorphous $CaAl_2Si_2O_8$. *Geochim. Cosmochim. Acta* **65**, 4019–4041.

Moulton K. L., West J. and Berner R. A. (2000) Solute flux and mineral mass balance approaches to the quantification of plant effects on silicate weathering. *Am. J. Sci.* **300**, 539–570.

Mungall J. E. and Martin R. F. (1994) Severe leaching of trachytic glass without devitrification, Terceira, Azores. *Geochim. Cosmochim. Acta* **58**, 75–83.

Oelkers E. H. (2001) General kinetic description of multioxide silicate mineral and glass dissolution. *Geochim. Cosmochim. Acta* **65**, 3703–3719.

Oelkers E. H. and Gislason S. R. (2001) The mechanism, rates, and consequences of basaltic glass dissolution: I. An experimental study of the dissolution rates of basaltic glass as a function of aqueous Al, Si, and oxalic acid concentration at 25 °C and pH = 3 and 11. *Geochim. Cosmochim. Acta* **65**, 3703–3719.

Oelkers E. H. and Schott J. (1995) Experimental study of anorthite dissolution and the relative mechanism of feldspar hydrolysis. *Geochim. Cosmochim. Acta* **59**, 5039–5053.

Oelkers E. H. and Schott J. (1999) Experimental study of kyanite dissolution rates as a function of chemical affinity and solution composition. *Geochim. Cosmochim. Acta* **63**, 785–797.

Oelkers E. H. and Schott J. (2005) Geochemical Aspects of CO_2 Sequestration. *Chem. Geol.* **217**, 183–186.

Oelkers E. H., Schott J. and Devidal J. L. (1994) The effect of aluminum, pH, and chemical affinity on the rates of aluminosilicate dissolution reactions. *Geochim. Cosmochim. Acta* **58**, 2011–2024.

Oelkers E. H., Gislason S. R. and Matter J. (2008) Mineral Carbonation of CO_2. *Elements* **4**, 333–337.

Oelkers E. H., Golubev S. V., Chairat C., Pokrovsky O. S. and Schott J. (2009) The surface chemistry of multi-oxide silicates. *Geochim. Cosmochim. Acta* **73**, 4617–4634.

Oelkers E. H., Gislason S. R., Eiriksdottir E. S., Jones M. T., Pearce C. R. and Jeandel C. (2011) The role of riverine particulate material on the global cycles of the elements. *Appl. Geochem.* **26**, S365–S369.

Parkhurst D.L. and Appelo C.A.J. (1999) User's guide to PHREEQC (Version 2) – a computer program for speciation, batch-reaction, one-dimensional transport, and inverse geochemical calculations. In *U.S. Geological survey Techniques of Water-Resources Investigation*, USGS, Restin, VA, USA, pp. 99–4259.

Petit J. C. (1992) Natural analogues for the design and performance assessment of nuclear radioactive waste form: a review. *J. Chem. Exp.* **46**, 1–33.

Pierce E. M., Reed L. R., Shaw W. J., McGrail P. B., Icenhower J. P., Windisch C. F., Cordova E. A. and Broady J. (2010) Experimental determination of the effect of the ratio of B/Al on glass dissolution along the nepheline($NaAlSiO_4$)–alinkoite ($NaBSiO_4$) join. *Geochim. Cosmochim. Acta* **74**, 2634–2654.

Powel P. E., Cline G. R., Reid C. P. P. and Stanizlo P. J. (1980) Ocurrence of hydroxymate siderophore iron chelators in soils. *Nature* **287**, 128–130.

Putnis A. (2009) Mineral replacement reactions (2009. *Rev. Min. Geochem.* **70**, 87–124.

Prapaipong P., Shock E. L. and Koretsky C. M. (1999) Metal–organic complexes in geochemical processes: temperature dependence of the standard thermodynamic properties of aqueous complexes between meal cations and dicarboxylate ligands. *Geochim. Cosmochim. Acta* **63**, 2547–2577.

Rajmohan N., Fruger P. and Gin S. (2010) Composition effects on synthetic glass alteration mechanism: Part 1. Experiments. *Chem. Geol.* **279**, 106–119.

Riley J. P. and Chester R. (1971) *Introduction to Marine Chemistry*. Academic Press.

Ruggieri F., Saavedra J., Fernandez-Turiel J. L., Gimeno D. and Garica-Valles (2010) Environmental geochemistry of ancient volcanic ashes. *J. Hazard. Mater.* **183**, 353–365.

Ruiz-Agudo E., Putnis C. V., Rodriguez-Navarro C. and Putnis A. (2012) Mechanism of leached layer formation during chemical weathering of silicate minerals. *Geology* **40**, 947–950.

Schott J. and Oelkers E. H. (1995) Dissolution and crystallization rates of silicate minerals as a function of chemical affinity. *Pure Appl. Chem.* **67**, 903–910.

Schott J., Pokrovsky O. S. and Oelkers E. H. (2009) The link between mineral dissolution/precipitation kinetics and solution chemistry. *Rev. Min. Geochem.* **70**, 207–258.

Shoesmith D. W. (2000) Fuel corrosion processes under waste disposal conditions. *J. Nucl. Mater.* **282**, 1–31.

Sparks R. S. J., Bursik M. I., Ablay G. J., Thomas R. M. E. and Carey S. N. (1992) Sedimentation of tephra by volcanic plumes. 2. Controls of thickness and grain-size variations of tephra fall deposits. *Bull. Volcanol.* **54**, 685–695.

Spivack A. J. and Staudigel H. (1994) Low-temperature alteration of the upper oceanic crust and the alkalinity budget of seawater. *Chem. Geol.* **115**, 239–247.

Stefansson A. and Gislason S. R. (2001) Chemical weathering of basalts, Southwest Iceland: effect of rock crystallinity and secondary minerals on chemical fluxes to the ocean. *Am. J. Sci.* **301**, 513–556.

Stewart C., Johnston D., Lenoard G. S., Horwell C. J., Thordson T. and Cronin S. J. (2006) Contamination of water supplies by volcanic ashfall: a literature review and simple impact model. *J. Volcanol. Geotherm. Res.* **158**, 296–306.

Techer I. (1999) Apports des analogues naturels vitreux a la validation des codes de prédiction du comportement a long terme des verres nucléaires. Thèse de doctorat, Montpellier II.

Techer I., Advocat T., Lancelot J. and Liotard J. M. (2001) Dissolution kinetics of basaltic glasses control by solution chemistry and protective effect of the alteration film. *Chem. Geol.* **176**, 235–263.

Thomassin J. H. and Touray J. C. (1979) Early stages of water-basaltic glass interaction – X-ray photo-electrons spectroscopy (XPS) and scanning electron-microscopy (SEM) investigations. *Bull. Miner.* **102**, 594–599.

Urey H. C. (1952) The origin and development of the earth and other terrestrial planets: a correction. *Geochim. Cosmochim. Acta* **2**, 263–268.

Wall-Palmer D., Jones M. T., Hart M. B., Fisher J. K., Smart C. W., Henbury D. J., Palmer M. R. and Fones G. R. (2011) Explosive volcanism as a cause for mass mortality of pteropods. *Mar. Geol.* **282**, 231–239.

White A. F. (1983) Surface chemistry and dissolution kinetics of glassy rocks at 25 °C. *Geochim. Cosmochim. Acta* **47**, 805–815.

White A. F. and Claassen H. C. (1980) Kinetic model for the short-term dissolution of a rhyolitic glass. *Chem. Geol.* **28**, 91–109.

Wilson T., Stewart C., Cole J., Johnston D. and Cronin S. (2010) Vulnerability of farm water supply systems to volcanic ash fall. *Environ. Earth Sci.* **61**, 675–688.

Wolff-Boenisch D., Gislason S. R., Oelkers E. H. and Putnis C. V. (2004a) The dissolution rates of natural glasses as a function of their composition at pH 4 and 10.6, and temperatures from 25 to 74 °C. *Geochim. Cosmochim. Acta* **68**, 4843–4858.

Wolff-Boenisch D., Gislason S. R. and Oelkers E. H. (2004b) The effect of fluoride on the dissolution rates of natural glasses at pH 4 and 25 °C. *Geochim. Cosmochim. Acta* **68**, 4571–4582.

Wolff-Boenisch D., Gislason S. R. and Oelkers E. H. (2006) The effect of crystallinity on dissolution rates and CO_2 consumption capacity of silicates. *Geochim. Cosmochim. Acta* **70**, 858–870.

Wolff-Boenisch D., Wenau S., Gislason S. R. and Oelkers E. H. (2011) Dissolution of basalts and peridote in seawater, in the presence of ligands, and CO_2: implication for mineral sequestration of carbon dioxide. *Geochim. Cosmochim. Acta* **75**, 5510–5525.

Yokoyama T. and Banfield J. F. (2002) Direct determinations of the rates of rhyolite dissolution and clay formation over 52,000 years and comparison with laboratory measurements. *Geochim. Cosmochim. Acta* **66**, 2665–2681.

Associate editor: Roy A. Wogelius